Dynamic myosin phosphorylation regulates contractile pulses and tissue integrity during epithelial morphogenesis

Claudia G. Vasquez, Mike Tworoger, and Adam C. Martin

Department of Biology, Massachusetts Institute of Technology, Cambridge, MA 02142

Apical constriction is a cell shape change that promotes epithelial bending. Activation of non-muscle myosin II (Myo-II) by kinases such as Rho-associated kinase (Rok) is important to generate contractile force during apical constriction. Cycles of Myo-II assembly and disassembly, or pulses, are associated with apical constriction during *Drosophila melanogaster* gastrulation. It is not understood whether Myo-II phospho-regulation organizes contractile pulses or whether pulses are important for tissue morphogenesis. Here, we show that Myo-II pulses are associated with pulses of apical Rok. Mutants that mimic Myo-II light chain phosphorylation or depletion of myosin phosphatase inhibit Myo-II contractile pulses, disrupting both actomyosin coalescence into apical foci and cycles of Myo-II assembly/disassembly. Thus, coupling dynamic Myo-II phosphorylation to upstream signals organizes contractile Myo-II pulses in both space and time. Mutants that mimic Myo-II phosphorylation undergo continuous, rather than incremental, apical constriction. These mutants fail to maintain intercellular actomyosin network connections during tissue invagination, suggesting that Myo-II pulses are required for tissue integrity during morphogenesis.

Introduction

Epithelial morphogenesis is critical for organs and embryos to change shape during development (Leptin, 2005; Heisenberg and Bellaïche, 2013). A cell shape change that often accompanies epithelial remodeling is apical constriction, which promotes epithelial sheet bending and cell invagination (Sawyer et al., 2010; Martin and Goldstein, 2014). One example of apical constriction–induced tissue remodeling occurs in *Drosophila melanogaster* gastrulation, when a group of ~1,000 cells along the ventral midline of the embryo undergoes apical constriction to form a ventral furrow. These constricted cells invaginate to become the mesoderm (Fig. 1 A; Leptin and Grunewald, 1990; Sweeton et al., 1991). The molecular motor nonmuscle myosin II (Myo-II), which localizes apically in *Drosophila* ventral furrow cells and other cell types that undergo apical constriction, is thought to generate the contractile force that facilitates invagination (Young et al., 1991; Nance et al., 2003; Dawes-Hoang et al., 2005; Hildebrand, 2005; Lee et al., 2006; Lee and Harland, 2007; Nishimura and Takeichi, 2008; Martin et al., 2009). Although

Myo-II is clearly involved in apical constriction, the mechanism of apical actomyosin contraction remains poorly understood.

Myo-II activity is regulated by phosphorylation of its regulatory light chain (RLC; *sqh* in *Drosophila*), which promotes Myo-II oligomerization into minifilaments and activation of the Myo-II motor ATPase activity (Karess et al., 1991; Sellers, 1991; Jordan and Karess, 1997). An effector of the RhoA GTPase (Rho1 in *Drosophila*), Rho-associated coiled-coil kinase (or Rho-associated kinase [Rok] in *Drosophila*), can phosphorylate and activate Myo-II via direct RLC phosphorylation or by inhibiting the phosphatase that dephosphorylates the RLC (myosin phosphatase; Amano et al., 1996; Kimura et al., 1996; Kawano et al., 1999; Winter et al., 2001). In the *Drosophila* mesoderm, the transcription factors Twist and Snail are thought to promote apical constriction and apical Myo-II accumulation by activating Rho1 and its effectors, including Rok (Barrett et al., 1997; Häcker and Perrimon, 1998; Dawes-Hoang et al., 2005; Fig. S1 A). Mutants or chemical inhibition of Rok results in loss of apical

The Rockefeller University Press $30.00
J. Cell Biol. Vol. 206 No. 3 435–450
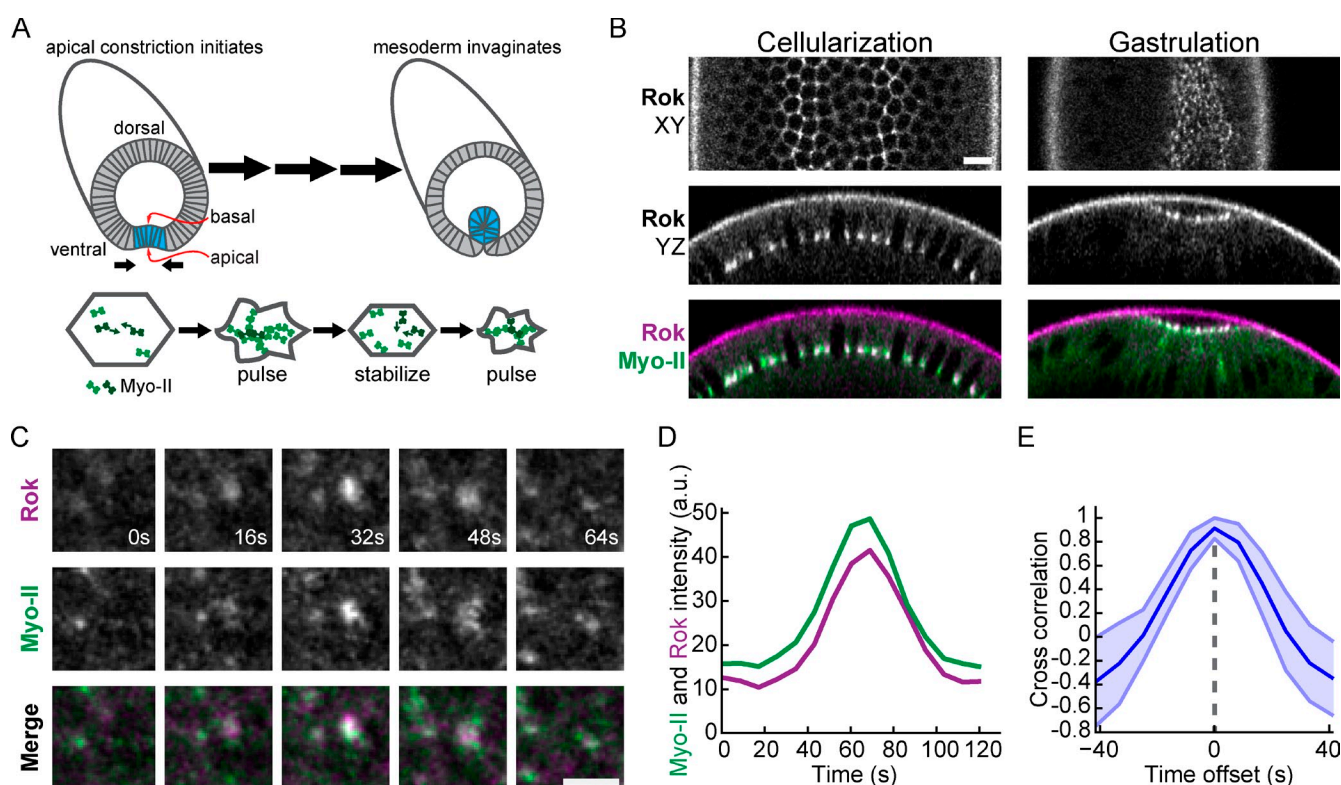www.jcb.org/cgi/doi/10.1083/jcb.201402004

JCB **435**

Figure 1. **Rok colocalizes with Myo-II pulses.** (A) Schematic of apical constriction of prospective mesodermal cells (shaded in blue) during *Drosophila* ventral furrow formation. (bottom) An individual cell undergoes pulsatile apical constriction. Myo-II undergoes cycles of assembly and coalescence (indicated by arrows) followed by remodeling. (B) Rok localizes with Myo-II at furrow canals during cellularization and apically (apical is up in YZ cross sections) during ventral furrow formation. Bar, 10 µm. (C) Time-lapse images of Rok and Myo-II intensity during a pulse from *rok²; Venus::Rok (WT); sqh::mCherry* embryo. Bar, 5 µm. (D) Myo-II and Rok appear simultaneously during pulse. Graph represents signal intensity of Rok and Myo-II within a single pulse event. (E) Rok signal is correlated with Myo-II signal with no temporal lag. Mean cross-correlation for different time offsets between Rok and Myo-II signals from pulses (*n* = 30 pulses; shaded area is ±SD).

Myo-II and lack of apical constriction, demonstrating that Rok is necessary for cortical Myo-II localization in the ventral furrow (Dawes-Hoang et al., 2005; Mason et al., 2013). In addition, mutants that mimic Myo-II RLC phosphorylation progress through development and suppress *rok* mutants, suggesting that Rok increases levels of active Myo-II to promote actomyosin contractility and morphogenesis (Jordan and Karess, 1997; Winter et al., 2001; Royou et al., 2002). It is not clear, however, whether coupling of Rok activity to Myo-II activation plays a role in organizing apical actin network contraction.

We have developed a system to visualize the dynamics of actomyosin contraction and apical constriction during *Drosophila* gastrulation. In ventral furrow cells, Myo-II undergoes cycles of assembly in the center of the apical surface (medioapical cortex) followed by disassembly or remodeling, which we refer to as pulses (Martin et al., 2009; Fig. 1 A). Phases of rapid apical constriction are associated with pulses of Myo-II assembly and the coalescence of Myo-II and F-actin structures into medioapical foci, which possibly represent contractions of the actin cortex (Martin et al., 2009; Roh-Johnson et al., 2012). After Myo-II coalescence, Myo-II structures remodel by either disassembling or changing in morphology. Despite Myo-II remodeling, cell shape is often stabilized between pulses, resulting in incremental apical constriction. Although Myo-II still undergoes pulsing in Twist knockdowns, the contracted cell shape

after a pulse is not stabilized, resulting in cell shape fluctuations and inefficient constriction (Martin et al., 2009, 2010). Thus, one model for ventral furrow formation is that cells undergo ratcheted apical constriction, whereby pulses drive constrictions that are stabilized via a Twist-dependent mechanism for efficient apical constriction. We proposed that the polarized localization of Rok to medioapical foci results in the persistence of medioapical actomyosin fibers that stabilize cell shape between pulses; we have named this cellular organization radial cell polarity (Mason et al., 2013). The persistence of medioapical Myo-II fibers is important for the formation of a supracellular Myo-II meshwork that transmits tension across the ventral furrow tissue (Martin et al., 2010). However, the roles of Rok and Myo-II phosphorylation during pulsatile constriction are still unclear. Furthermore, it is not known why cells undergo pulsatile rather than continuous contraction to promote tissue morphogenesis.

Here, we combined live imaging and quantitative analysis of Myo-II regulators and GFP-tagged Myo-II RLC phosphomutants to define the role of coupling Myo-II activation to upstream signals during contractile pulses. We show that temporal and spatial control of Myo-II phosphorylation organizes contractile pulses. We suggest that the pulsatile nature of apical constriction is required for the stable transmission of intercellular forces during tissue morphogenesis.

Results

Myo-II pulses correlate with fluctuations in apical Rok localization

Contractile pulses during ventral furrow cell apical constriction are associated with the coalescence and increase in apical Myo-II intensity, after which apical Myo-II structures are remodeled (Fig. 1 A; Martin et al., 2009). Because Rok is required for cortical Myo-II localization in the *Drosophila* embryo (Royou et al., 2002; Dawes-Hoang et al., 2005), we examined whether dynamic Myo-II localization was correlated with changes in Rok localization. Before gastrulation, Rok localizes to basal furrow canals and is relocalized to foci in the center of the apical domain during apical constriction (Mason et al., 2013; Fig. 1 B). At the onset of apical constriction, we found that Rok intensity exhibited clear fluctuations, with medioapical Rok foci appearing and disappearing in association with Myo-II coalescence (Fig. 1, C and D; and Video 1). Analysis of the time-resolved cross-correlation between Myo-II and Rok intensity during individual pulses demonstrated a significant correlation that peaked at 0 s offset (Fig. 1 E). Thus, Myo-II foci appear at the same time as Rok foci. Additionally, apical Rok intensity increased during apical constriction, often in bursts that corresponded with phases of rapid constriction (Fig. S1 B). The pulsatile behavior of Rok during ventral furrow formation suggests that dynamic changes in Myo-II phosphorylation by Rok direct contraction pulses that result in incremental apical constriction.

RLC mutants that mimic mono- or diphosphorylation result in constitutive Myo-II oligomerization independent of Rok

To test whether dynamic Myo-II phosphorylation, and thus changes in Myo-II minifilament assembly and motor activity, is required for Myo-II pulses, we generated GFP-tagged *sqh* mutants affecting threonine-20 and serine-21 (Fig. 2 A; Jordan and Karess, 1997). Alanine substitutions in these residues decrease Myo-II motor ATPase activity in vitro (Kamisoyama et al., 1994), and the *sqh-AA* mutant resembles a *sqh* null allele in vivo (Jordan and Karess, 1997). Conversely, glutamate substitutions activate Myo-II minifilament assembly and ATPase activity in the absence of phosphorylation in vitro, although the ATPase activity of phosphomimetic myosin mutants is lower than that of phosphorylated Myo-II (Kamisoyama et al., 1994). We differentiated between possible roles of mono- and diphosphorylation by generating mutants that trap the Myo-II motor in all possible combinations of RLC phosphorylation states that are likely present in vivo (Fig. 2 B). The *sqh* phosphomutants were expressed at similar levels as endogenous *sqh* and did not exhibit gastrulation phenotypes in the presence of the endogenous Sqh (Figs. S1 C and S2 A). We reduced endogenous Sqh protein levels ∼90% by making germline clones with the hypomorphic *sqh[1]* allele (Fig. S1, C and D). The wild-type *sqh* transgene (*sqh-TS::GFP*), but not the inactive *sqh-AA::GFP* allele, rescued nuclear migration and the uneven cellularization phenotypes of *sqh[1]* mutants (Fig. 2 C; Wheatley et al., 1995; Royou et al., 2002, 2004). In addition, we obtained gastrulating embryos from all mutants, including the *sqh-AA* allele. Thus, the partial activity of the *sqh[1]*

allele enabled us to examine the function of *sqh* phosphomutants during gastrulation.

We first determined whether the different *sqh* phosphomimetic mutants activate Myo-II minifilament assembly in vivo. During cellularization, Myo-II localizes to basal furrow canals and cytoplasmic aggregates (Royou et al., 2004). Although we did not observe ectopic cortical Myo-II assembly, phosphomimetic *sqh* mutants, particularly *sqh-AE* and *sqh-EE*, accumulated Myo-II in aggregates that are immediately basal to the furrow canals (Fig. 2 C and Fig. S1 E). Myo-II aggregates were reduced in size when wild-type levels of endogenous Sqh were present and Myo-II aggregates also contained the myosin heavy chain (*Drosophila zipper*), suggesting that these aggregates are not denatured protein (Fig. 2, C and D). Importantly, Sqh aggregates do not contain F-actin, suggesting that the Sqh aggregates do not form by actomyosin contraction, but could result from constitutive Myo-II minifilament assembly (Fig. 2 E). The phosphomimetic mutants resulted in a decrease in cytoplasmic Myo-II levels relative to wild-type embryos, suggesting that RLC mutants that mimic mono- or diphosphorylation shift the Myo-II complex toward the active conformation in vivo, promoting constitutive oligomerization (Fig. 2 F). Thus, our GFP-tagged phosphomimetic RLC mutants appear to uncouple activation of Myo-II oligomerization from phosphorylation by Rok.

RLC phosphorylation dynamics do not trigger changes in Myo-II apical–basal localization

Apical activation of Rok has been proposed to localize Myo-II assembly during apical constriction (Dawes-Hoang et al., 2005). Thus, mutants that uncouple Myo-II activity from phosphorylation by Rok might disrupt the apical–basal localization of Myo-II. Therefore, we tested whether the apical–basal polarity of Myo-II localization is controlled by RLC phosphorylation and oligomerization. Mutants that mimic mono- or diphosphorylation localized specifically to the apical surface of ventral furrow cells, despite the presence of Myo-II aggregates throughout the entire embryo during cellularization (Fig. 3, A and B; Fig. S2 B; and Video 2). Furthermore, Myo-II was reduced in basal furrow canals during ventral furrow invagination in phosphomimetic mutants, similar to wild-type Myo-II, suggesting that dephosphorylation of the RLC is not the mechanism of basal Myo-II loss (Fig. 3, A and B). Inactivation of the RLC phosphorylation sites similarly did not disrupt apical Myo-II localization (Fig. 3 C, Fig. S2 B, and Video 2). These results demonstrate that despite the tissue-specific apical recruitment of Rok in ventral furrow cells, regulation of oligomerization does not instruct apical Myo-II localization at the onset of gastrulation.

Phosphomimetic RLC mutants disrupt polarized actomyosin condensation

Medioapical Myo-II pulses involve the coalescence or condensation of both Myo-II and F-actin into medioapical foci (Martin et al., 2009; Mason et al., 2013). Because Rho1 and Rok are also enriched in medioapical foci, we have proposed that the apical domain of ventral furrow cells exhibits radial cell polarity, with protein localization differing between the apical center
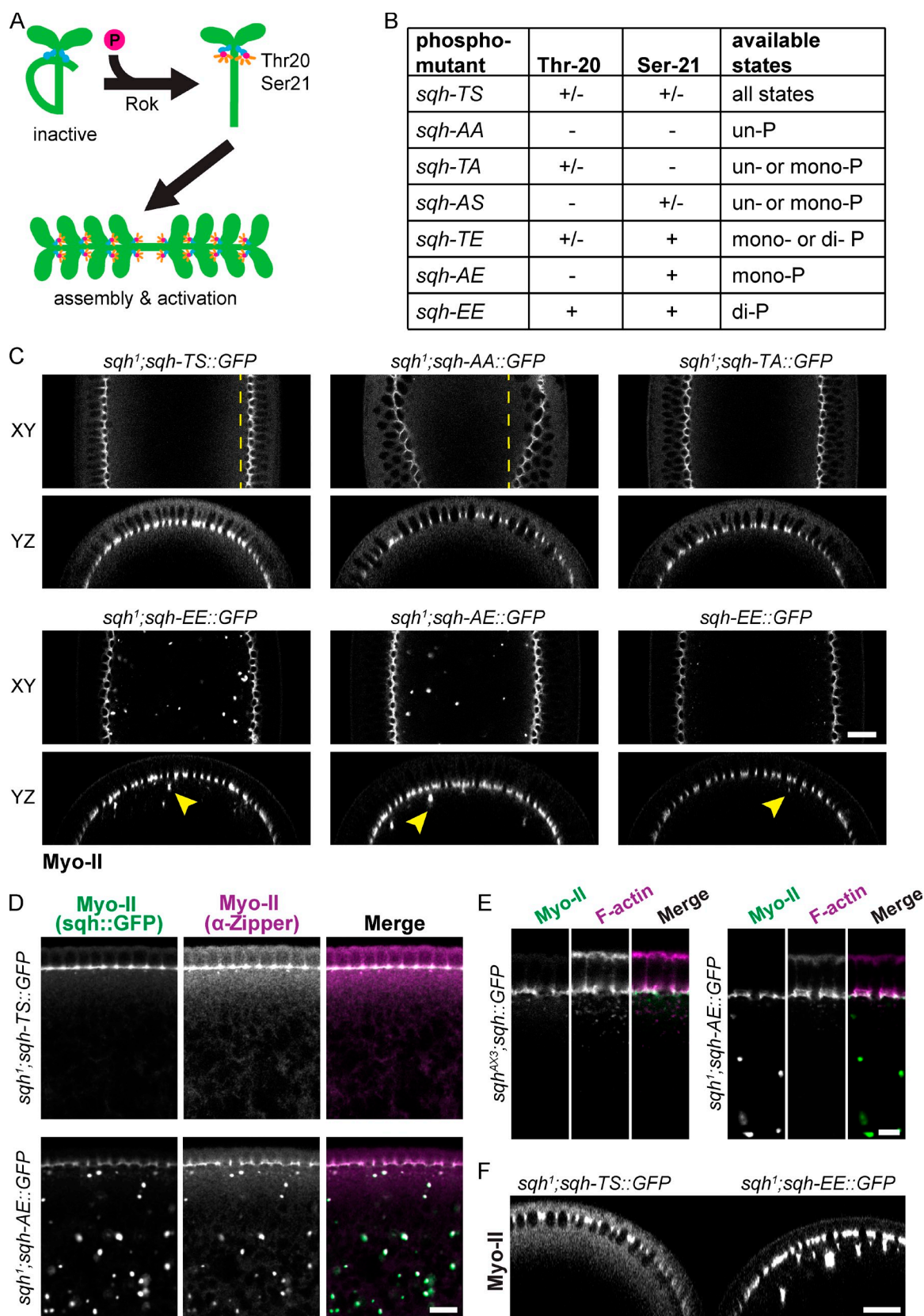
Figure 2. **Characterization of *sqh* phosphomutant oligomerization.** (A) Phosphorylation of the *Drosophila* Myo-II RLC *sqh* on threonine-20 and serine-21 is predicted to activate motor activity and promote bipolar minifilament assembly. (B) Chart summarizing phosphorylation states available to different Sqh phosphomutants. (C) Sqh mutants that mimic phosphorylation result in cytoplasmic Myo-II aggregates. Representative images of XY semisagittal sections and YZ cross sections for live cellularizing embryos. Dashed lines highlight evenness (*sqh-TS*) or unevenness (*sqh-AA*) of cellularization front. Arrowheads indicate examples of cytoplasmic Myo-II aggregates. Bar, 20 μm. (D) Basal Sqh aggregates colocalize with Zipper aggregates. Images are fixed embryos
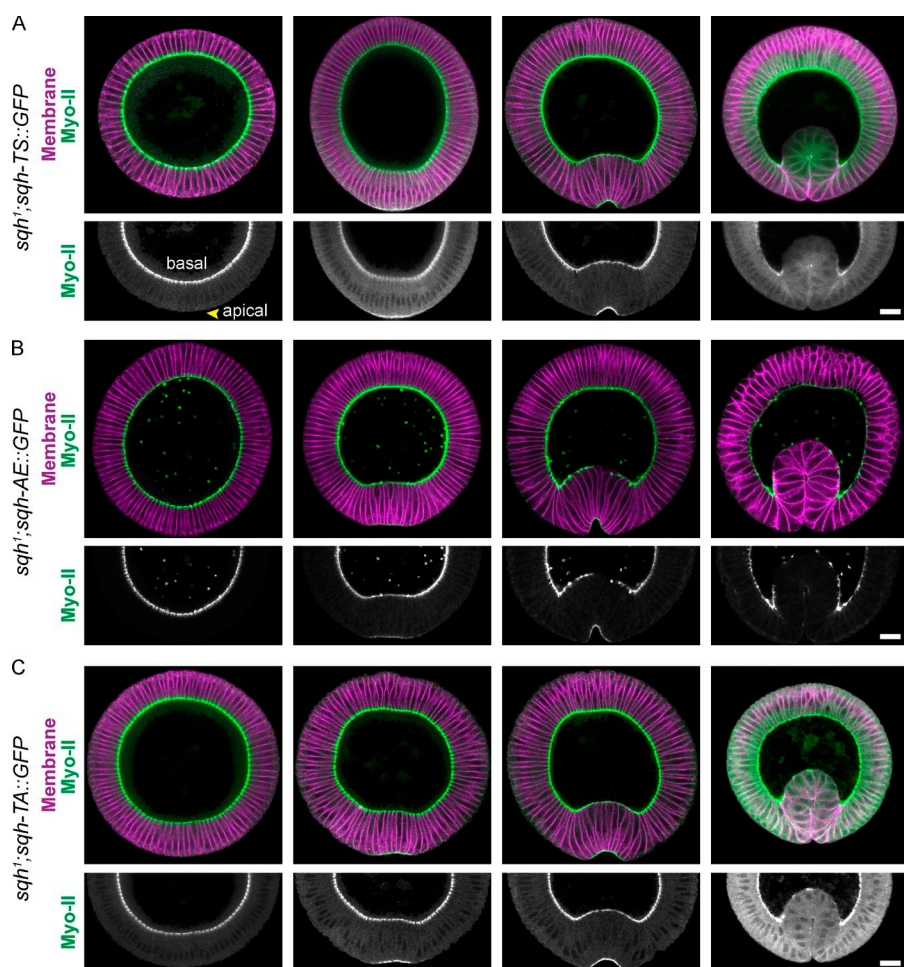
Figure 3. **Dynamic RLC phosphorylation is not required to trigger basal to apical relocalization of Myo-II.** (A) Wild-type Myo-II localizes to the apical surface and is reduced basally during ventral furrow formation. Images are fixed embryo cross sections during sequential stages of apical constriction stained for Zipper (myosin heavy chain) and neurotactin (membrane). (B and C) Sqh phosphomutants do not alter the basal–apical Myo-II redistribution. Embryo preparation was the same as in A, except germline clones expressing *sqh-AE* (B) and *sqh-TA* (C) were fixed. Bars, 20 µm.

to the junctions (Mason et al., 2013). To test whether dynamic regulation of RLC phosphorylation polarizes actomyosin within the apical cortex, we combined *sqh::GFP* transgenes with a membrane marker fused to mCherry (Memb::Cherry) to visualize and quantify the apical organization of Myo-II. Because we have been unable to obtain viable embryos expressing Memb::Cherry and *sqh-EE::GFP*, which exhibits additional oogenesis defects associated with constitutive Myo-II activation, we focused our quantitative analysis on the *sqh-AE* mutant. We observed similar Myo-II localization and mutant phenotypes between *sqh-AE* and *sqh-EE*, consistent with these mutants similarly activating Myo-II oligomerization. The *sqh-TS::GFP* transgene rescued Myo-II coalescence in *sqh¹* germline clone mutants, forming medioapical foci during pulses and thus exhibiting radial cell polarity in Myo-II accumulation (Fig. 4 A). In contrast, Myo-II in *sqh-AE* mutants accumulated across the entire apical domain, at both the junctional and the medioapical cortex, but failed to coalesce (Fig. 4 B). Consistent with the defect in Myo-II coalescence, the *sqh-AE* mutant also failed to condense apical F-actin during Myo-II accumulation (Fig. 4, E and F; and Video 3). We quantified this difference in the radial cell polarity of Myo-II

localization by calculating the difference between medioapical and junctional/peripheral Myo-II intensity before and after the onset of apical constriction. Because wild-type Myo-II coalesces toward the center of the medioapical cortex, the amount of medioapical Myo-II relative to peripheral Myo-II increases when cells begin constricting (Medioapical polarity >0; Fig. 4 D). In contrast, Myo-II in the *sqh-AE* mutant did not exhibit this medioapical enrichment, indicating a defect in medioapical Myo-II coalescence (Fig. 4 D). The defect in the medioapical polarization of Myo-II was specific to phosphomimetic mutants because Myo-II in both the *sqh-AA* and *sqh-TA* mutants accumulated as concentrated foci and the *sqh-TA* mutant exhibited medioapical F-actin condensation (Fig. 4, C, D, and G; and Videos 2 and 3). Thus, the defects in actomyosin coalescence observed in the *sqh-AE* mutants suggest that coupling of Myo-II activation to Rok phosphorylation is critical to polarize actomyosin contractile activity within the apical domain of ventral cells.

Because Myo-II localization in the phosphomimetic mutants could be influenced by the low (10%) levels of endogenous Sqh, we sought to fully uncouple Myo-II activation from upstream signals by activating Myo-II in a *rok* mutant background. Either

stained for Zipper (myosin heavy chain) and endogenous GFP. Bar, 10 µm. (E) Basal Sqh aggregates do not colocalize with F-actin. Images are fixed embryos stained for F-actin (phalloidin) and endogenous GFP. Bar, 5 µm. (F) Phosphomimetic Sqh mutants deplete levels of cytoplasmic Myo-II. Image is a YZ cross section of a live *sqh¹*; *sqh-TS*::GFP embryo immediately adjacent to a *sqh¹*; *sqh-EE*::GFP embryo. Bar, 20 µm.
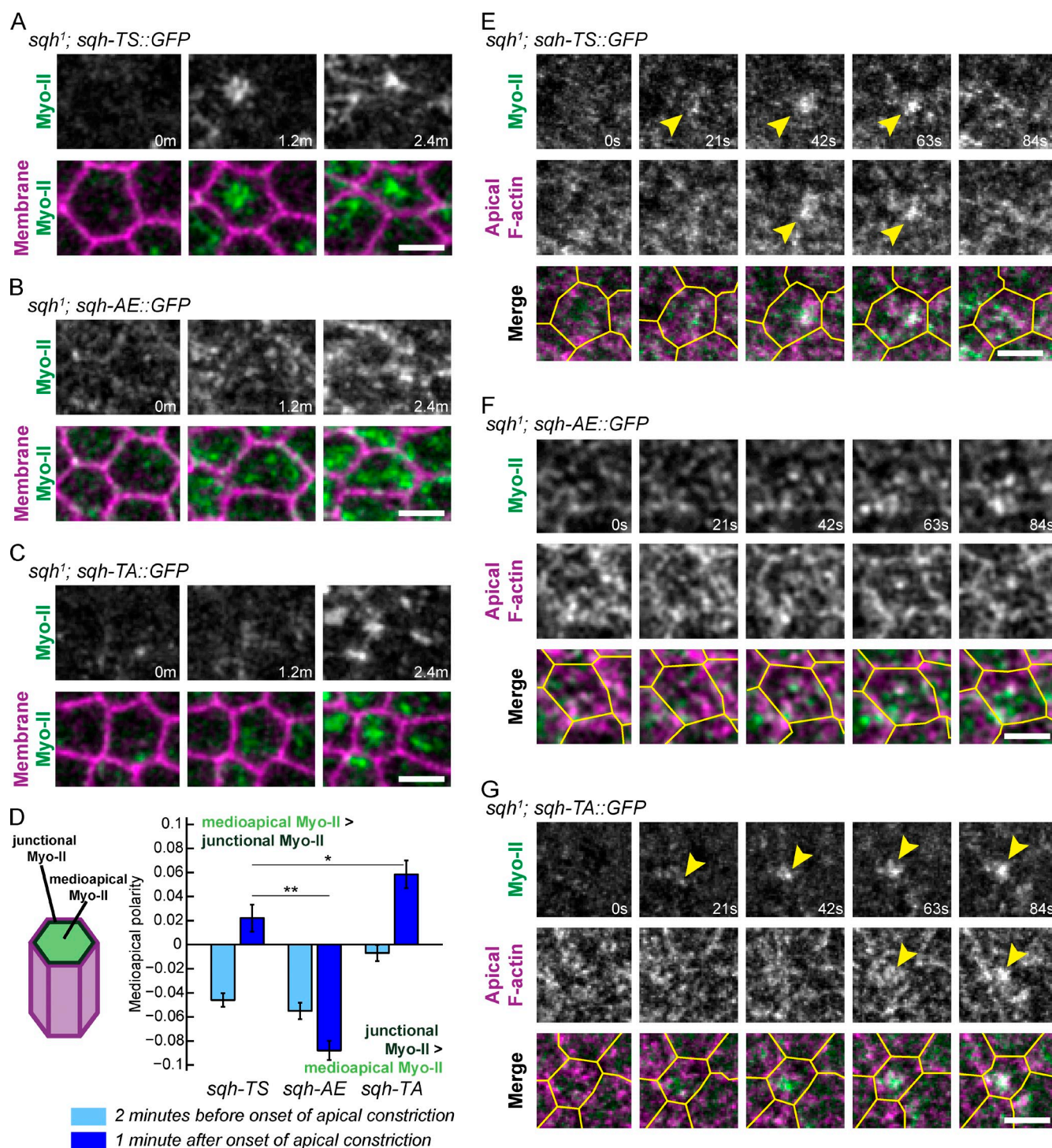
Figure 4. **Polarized actomyosin condensation requires dynamic Myo-II phosphorylation.** (A–C) Uncoupling Myo-II activation from Rok phosphorylation disrupts medioapical Myo-II coalescence. Time-lapse images are representative cells from sqh^1 germline clone embryos expressing the indicated phosphomutants and Memb::Cherry (membrane). Bars, 5 µm. (D) Quantification of Myo-II medioapical polarity, which is the difference between medioapical Myo-II (light green in schematic) and junctional Myo-II (green in schematic) intensities normalized by the total Myo-II intensity in a cell. Error bars are SEM ($n = 120$ sqh-TS cells, two embryos; $n = 100$ sqh-AE cells, two embryos; $n = 118$ sqh-TA cells, two embryos). (E–G) The sqh-AE mutant fails to condense apical F-actin. Time-lapse images are of representative cells from sqh^1 germline clone embryos expressing the indicated phosphomutants and Utr::mCherry (F-actin). Arrowheads indicate Myo-II and F-actin condensation. Cell outlines in yellow were made by manually segmenting the subapical Utr::mCherry signal 2 µm below the apical meshwork. Bars, 5 µm. *, P < 0.05; **, P < 0.01.

rok¹ or *rok²* mutant germline clones result in a loss of Myo-II from the cortex, consistent with Rok and Myo-II phosphorylation being required for Myo-II activation (Fig. S3 and Video 4; Royou et al., 2002; Dawes-Hoang et al., 2005; Mason et al., 2013). Previous studies suggested that *sqh-EE* can suppress loss of Rok function (Winter et al., 2001; Bertet et al., 2004), suggesting that Rok activates Myo-II minifilament assembly, whereras minifilament localization is dependent on other cortical cues. Consistent with these results, we found that *sqh-EE* rescued cortical Myo-II localization in *rok¹* and *rok²* mutant germline clones (Fig. S3). However, despite rescuing cortical localization in *rok* germline clones, *sqh-EE* Myo-II failed to undergo medioapical coalescence and generate cell contractions (Video 4). Instead, Myo-II accumulated uniformly across the apical domain (Fig. S3). Furthermore, the *rok sqh-EE* double mutants failed to undergo mesoderm invagination (Video 4). Although we cannot rule out the possibility that other Rok substrates are required for Myo-II coalescence, our data suggest that simply activating apical Myo-II is not sufficient for medioapical actomyosin network condensation and radial cell polarity. We favor a model whereby spatial regulation of Myo-II by Rok within the apical domain is required for actomyosin network contraction during a pulse.

Myo-II phosphomutants exhibit defects in Myo-II assembly/disassembly cycles

We next determined whether dynamic Myo-II phosphorylation is critical for temporal organization of Myo-II pulses. Similar to Myo-II in wild-type embryos, *sqh-TS::GFP* displayed Myo-II contraction pulses in *sqh¹* germline clones, with the appearance of Myo-II structures lasting 20 to 30 s before being disassembled or remodeled (Fig. 5 A). In contrast, phosphomimetic mutants caused a gradual increase in Myo-II accumulation (Figs. 5 B and S2 C). Myo-II persisted long after it initially appeared, failing to undergo disassembly over the course of constriction (Fig. 5 B and Video 5). Based on the frequency of events involving rapid Myo-II intensity increase, we found that the *sqh-AE* mutant had significantly fewer Myo-II pulses than wild-type embryos (Fig. 5 D). Correspondingly, apical constriction in the *sqh-AE* mutant appeared more continuous, with fewer rapid phases of constriction that were lower in magnitude than those observed in wild-type (Fig. 5, B, E, and F; and Fig. S4 A). During pulsatile constriction, phases of rapid Myo-II accumulation correlate with increased constriction rate (Martin et al., 2009). However, the *sqh-AE* mutant displayed a significantly weaker cross-correlation between Myo-II accumulation and the constriction rate, confirming our observation that mimicking Sqh phosphorylation disrupts contractile pulses and results in more continuous apical constriction (Fig. 5 G).

Mutants that decrease Myo-II phosphorylation resulted in Myo-II dynamics that were distinct from the phosphomimetic alleles. The *sqh-AS* mutant displayed contractile oscillations and Myo-II disassembly similar to wild-type embryos (Fig. S2 C), suggesting that dynamic phosphorylation of serine-21 is sufficient for Myo-II remodeling. The *sqh-TA* mutant exhibited phases of rapid Myo-II accumulation that were temporally correlated with constriction (Fig. 5, C and G), which possibly results

from Rok phosphorylating threonine-20. However, the *sqh-TA* and *sqh-AA* mutants did not exhibit Myo-II disassembly after accumulation, demonstrating that dynamic phosphorylation of threonine-20 is insufficient for Myo-II remodeling (Fig. 5, C–G; and Figs. S2 C and S4 A). These data are consistent with in vitro experiments that show phosphorylation of either threonine-20 or serine-21 can promote minifilament formation, but that serine-21 is most important for Myo-II ATPase activity (Kamisoyama et al., 1994; Bresnick et al., 1995), suggesting that high levels of Myo-II motor activity are required to remodel the actomyosin network after a pulse. Thus, cycling between high and low Myo-II activity states is required for contractile oscillations.

Myosin phosphatase localizes to the Myo-II contractile network and is required for contractile pulses

Continuous Myo-II accumulation in the phosphomimetic mutants suggested that Myo-II dephosphorylation plays a critical role in remodeling Myo-II pulses. Myosin phosphatase is a multisubunit enzyme that includes a catalytic protein phosphatase 1cδ (PP1cδ; also referred to as PP1cβ in *Drosophila*) and a myosin-binding subunit (MBS) that targets PP1cβ to Myo-II (Hartshorne et al., 1998). Previous studies showed that the *Drosophila* homologues of MBS and PP1cβ regulate the phosphorylation state of Myo-II during multiple developmental stages (Tan et al., 2003; Ong et al., 2010; Sun et al., 2011; Majumder et al., 2012). Therefore, we determined whether MBS could catalyze the dynamic remodeling of Myo-II that occurs during pulsing. During cellularization, MBS localizes to Rok/Myo-II–containing furrow canals (Figs. 1 B and S1 F). In addition, MBS localizes to basal Myo-II particles in *sqh-TS* mutants and to basal aggregates in *sqh-AE* mutants, providing further evidence that phosphomimetic mutants convert Myo-II into an active conformation that undergoes oligomerization (Fig. S1 F). During ventral furrow formation, MBS is present in the apical cytoplasm of all cells and is enriched in the apical cortex of ventral furrow cells (Fig. 6 A). MBS colocalized with both apical Myo-II and Rok foci throughout the process of ventral furrow formation (Fig. 6, B and C). To determine whether MBS is required for Myo-II pulses, we knocked down MBS using maternal expression of a shRNA that targets MBS (Ni et al., 2011; Fig. S1 G). MBS knockdown resulted in apical Myo-II assembly that exhibited a defect in medioapical coalescence, reminiscent of Myo-II organization in phosphomimetic mutants (Fig. 6, D–F; and Video 6). Although periods of rapid Myo-II accumulation did occur in MBS knockdowns (Fig. 6 G), changes in Myo-II signal were not well correlated with constriction (Fig. 6 H). These data suggest that Myo-II dynamics in MBS knockdown cells is uncoupled from area constriction, indicating that there is a defect in the pulsing behavior compared with wild-type cells. Consistent with this atypical Myo-II behavior, cells in MBS knockdown embryos exhibited more persistent Myo-II accumulation and constriction (Fig. 6 E, Fig. S4 B, and Video 6). Thus, MBS is recruited to apical Myo-II where it is required to polarize Myo-II accumulation and to generate cycles of assembly and disassembly.
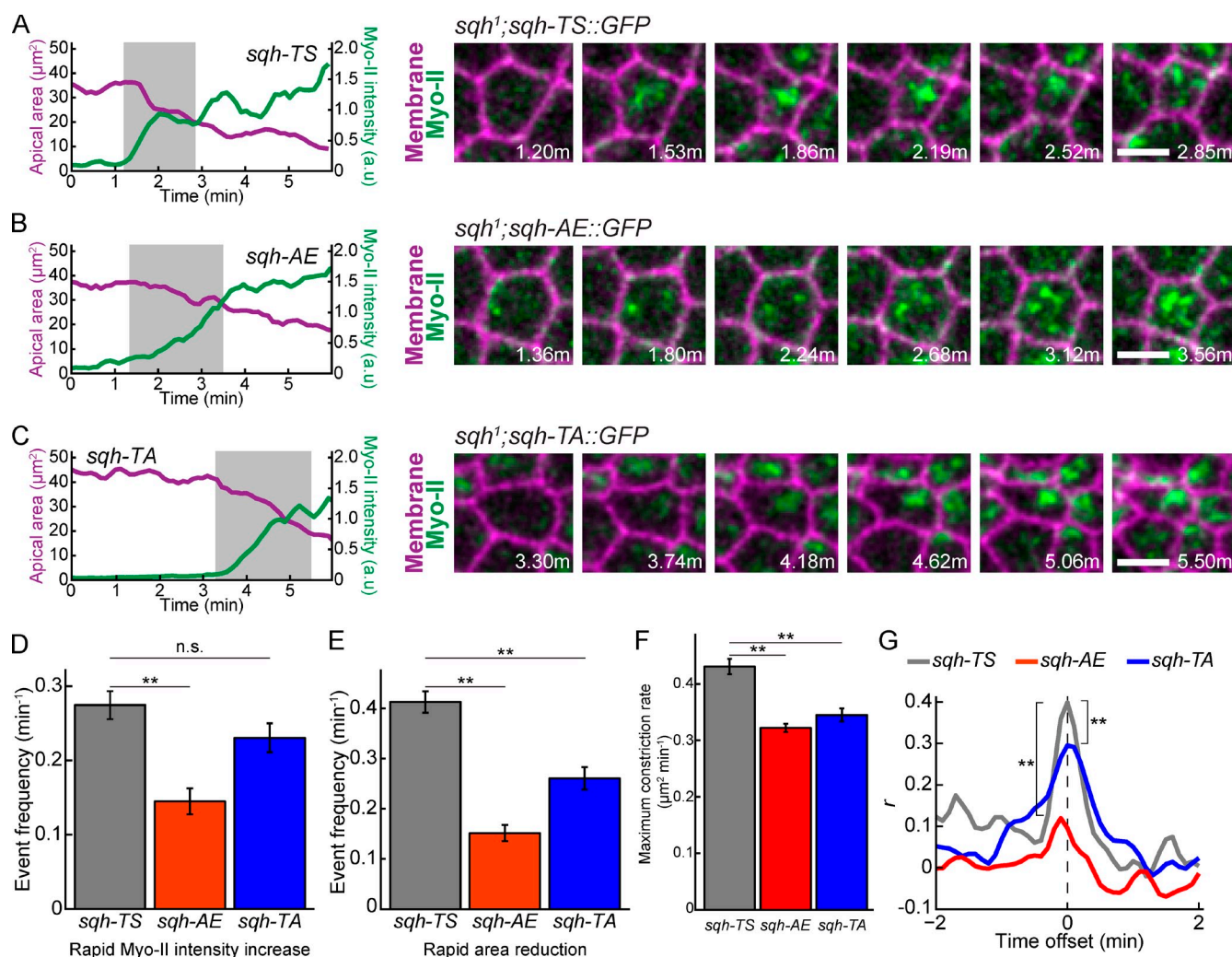
Figure 5. **Cycles of Myo-II assembly and disassembly require dynamic RLC phosphorylation.** (A–C) The *sqh-AE* and *sqh-TA* mutants inhibit Myo-II remodeling associated with pulses. Time-lapse images are representative cells from *sqh¹* germline clone embryos expressing the indicated phosphomutants and Memb::Cherry (membrane). Plots represent apical area and Myo-II intensity as a function of time for the same cells; the time highlighted in gray corresponds to the time time-lapse shown. Bars, 5 µm. (D) Quantification of frequency of instances where there is a rapid increase in Myo-II intensity (n = 94 *sqh-TS* cells, two embryos; n = 131 *sqh-AE* cells, three embryos; n = 92 *sqh-TA* cells, two embryos). (E) Quantification of frequency of instances of rapid apical area reduction (n = 94 *sqh-TS* cells, two embryos; n = 131 *sqh-AE* cells, three embryos; n = 92 *sqh-TA* cells, two embryos). (F) Quantification of maximal instantaneous constriction rate achieved in control or mutant cells (n = 138 *sqh-TS* cells, two embryos; n = 187 *sqh-AE* cells, three embryos; n = 172 *sqh-TA* cells, two embryos). (D–F) Error bars are SEM. (G) Mean cross-correlation between constriction rate and change in Myo-II intensity (n = 123 *sqh-TS* cells, two embryos; n = 143 *sqh-AE* cells, three embryos; n = 88 *sqh-TA* cells, two embryos). P-values were calculated at 0 time offset. **, P < 0.01; n.s., not significant.

Myo-II pulses are important for maintaining tissue integrity during morphogenesis

It is unknown why cells undergo pulsatile, rather than continuous, contraction during tissue morphogenesis. Because we were able to disrupt contractile pulses and promote more persistent apical Myo-II accumulation using both Myo-II phosphomutants and MBS depletion, we next investigated the consequences of continuous apical constriction on tissue invagination. Surprisingly, many of the phosphomutants that disrupted contractile pulses (with the exception of the *sqh-AA* mutant) underwent apical constriction and tissue invagination (Fig. 7, A–C; Fig. S5, A–C; and Video 2). On average, the *sqh-AE* mutant cells constricted more slowly than wild-type *sqh-TS* control cells, suggesting that unregulated Myo-II may decrease the rate of apical constriction and tissue invagination (Fig. 7, A and C; and

Fig. S5 B). However, phosphomimetic mutations in other Myo-II RLCs have been shown to not fully recapitulate the ATPase activity of phosphorylated Myo-II in vitro (Kamisoyama et al., 1994). Importantly, MBS depletion, which also appears to trap Myo-II in the phosphorylated state, resulted in apical constriction with similar rates to control cells, despite greater heterogeneity in cell size (Fig. 7, D–F). Thus, although contractile pulses may enhance constriction rate, they do not appear to be required for individual cell apical constriction.

Although apical constriction and tissue invagination occur in Sqh phosphomutants, the coordination of tissue invagination was perturbed. In wild-type ventral furrows, Myo-II foci in neighboring cells come together steadily to form a dense supracellular Myo-II meshwork across the entire tissue (Fig. 7 G and Video 7). Furrows in Myo-II phosphomimetic mutants underwent
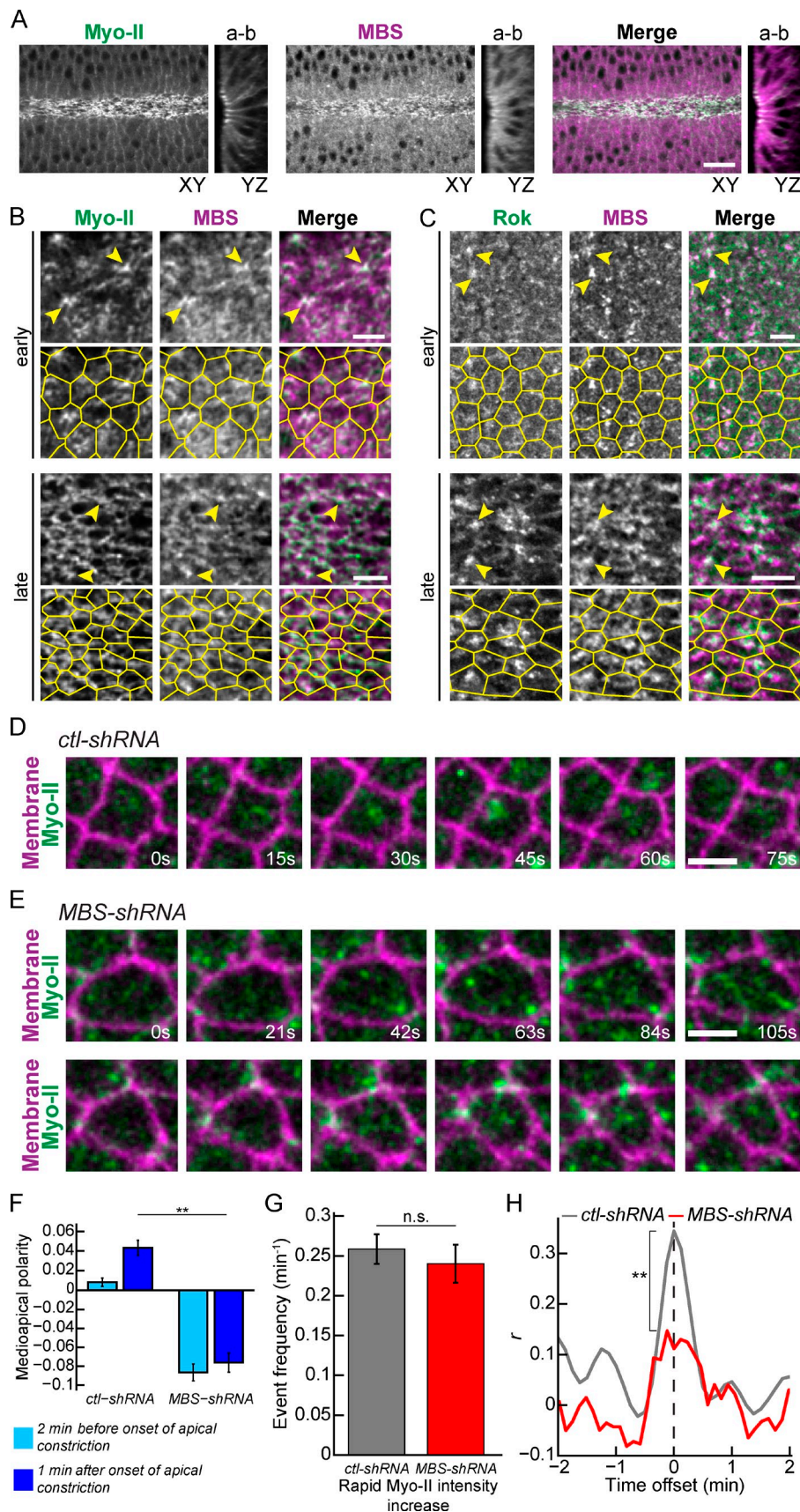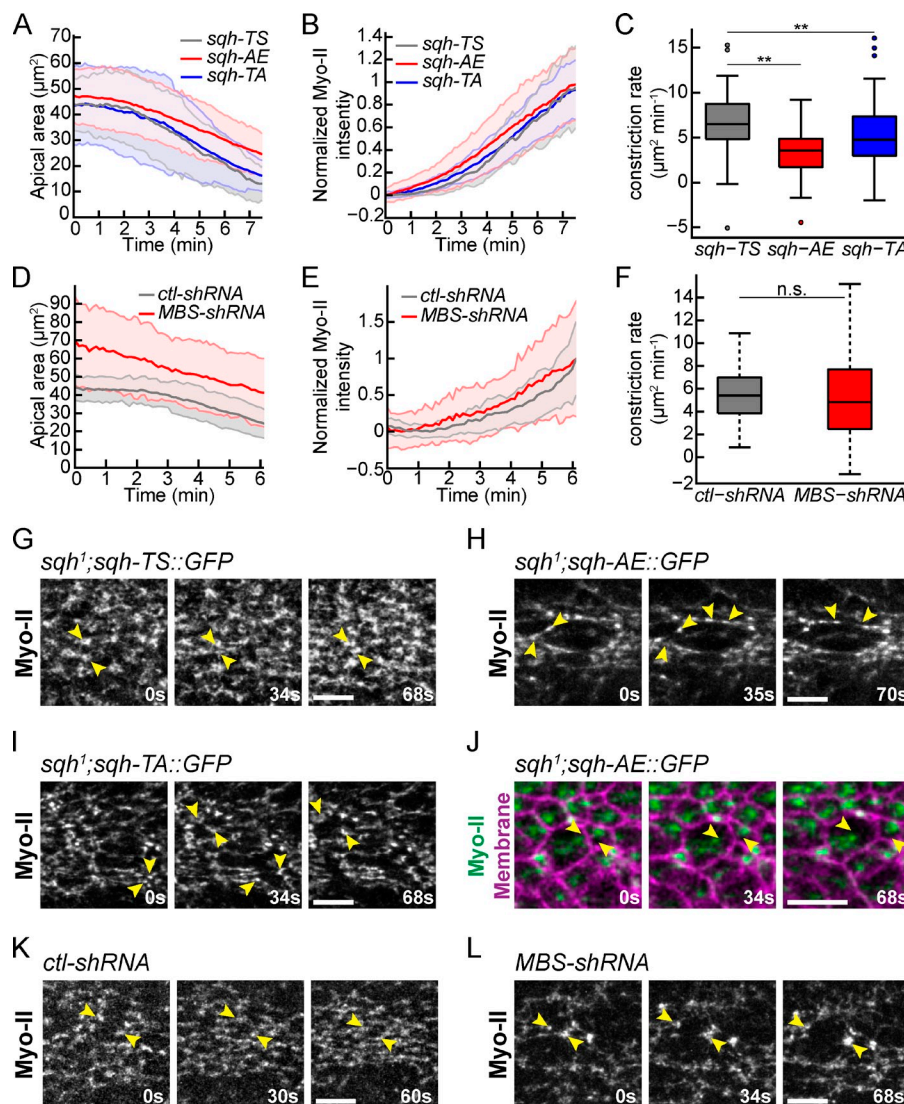
Figure 6. **Myo-II contractile pulses require MBS.** (A) MBS is apically enriched in ventral furrow cells. Images of XY semisagittal and YZ cross sections for fixed *sqh::GFP* embryos stained for MBS. Bar, 10 μm. (B) MBS structures colocalize with Myo-II foci and the supracellular Myo-II meshwork (arrowheads). Images are from fixed *sqh::GFP* embryos stained for MBS. Bars, 5 μm. Segmented cell outlines are from subapical *sqh::GFP* signal. (C) MBS colocalizes with Rok foci (arrowheads). Images are from fixed *GFP::Rok* embryos stained for MBS. Bars, 5 μm. Segmented cell outlines are from subapical Rok signal. (D and E) MBS knockdown inhibits Myo-II pulses. Time-lapse images are cells from embryos expressing *control-shRNA* (*ctl-shRNA*) (D) or *MBS-shRNA* (E), *sqh::GFP* (Myo-II), and Memb::Cherry (membrane). (F) Quantification of Medioapical polarity in Myo-II organization (n = 115 *ctl-shRNA* cells, two embryos; n = 123 *MBS-shRNA* cells, two embryos). Error bars are SEM. (G) Frequency of rapid increases of Myo-II intensity (n = 82 *ctl-shRNA* cells, two embryos; n = 70 *MBS-shRNA* cells, three embryos). Error bars are SEM. (H) Mean cross-correlation between constriction rate and change in Myo-II intensity for cells as a function of time offset (n = 118 *ctl-shRNA* cells, two embryos; n = 84 *MBS-shRNA* cells, three embryos). P-values were calculated at 0 time offset. **, P < 0.01; n.s, not significant.

Figure 7. **Defects in Myo-II pulsing disrupt the integrity of the supracellular actomyosin meshwork.** (A and B) Mean apical area (A) and normalized mean cellular Myo-II intensity (B) for representative *sqh¹* germline clone embryos expressing the indicated phosphomutants (n = 50 *sqh-TS* cells; n = 49 *sqh-TA* cells, and n = 50 *sqh-AE* cells). Shaded area is ±SD. (C) Box-and-whisker plot of cell constriction rates for multiple *sqh¹* germline clone embryos expressing the indicated phosphomutants (n = 102 *sqh-TS* cells, two embryos; n = 169 *sqh-AE* cells, three embryos; and n = 189 *sqh-TA* cells, three embryos). (D and E) Mean apical area (D) and normalized mean cellular Myo-II intensity (E) for representative embryos expressing the indicated shRNA (n = 78 *control-shRNA* cells; n = 31 *MBS-shRNA* cells). Apical area of cells in *MBS-shRNA* knockdown embryos were more heterogenous and larger than that of *ctl-shRNA* embryos; however, they undergo apical constriction. Shaded area is ±SD. (F) Box-and-whisker plot of constriction rates for multiple embryos expressing the indicated shRNA (n = 104 *control-shRNA* cells, two embryos; n = 78 *MBS-shRNA* cells, three embryos). (G–L) Myo-II phosphomutants and MBS knockdown cause separation of Myo-II networks between cells. Time-lapse images are of representative cells from *sqh¹* germline clone embryos with the indicated phosphomutants or from embryos expressing the indicated shRNA. Arrowheads indicate contraction of an intact supracellular Myo-II meshwork in control embryos (G and K) or instances of intercellular Myo-II network separation in mutants or knockdowns (H–J and L). Bars, 10 µm. Box-and-whisker plots display the median (central line), 25th and 75th percentiles (box edges), the most extreme data points not considered outliers (whiskers), and outliers (plotted individually). **, P < 0.01; n.s., not significant.

global contraction, but exhibited abnormal stretching of Myo-II networks and separation of Myo-II foci at late stages of furrow invagination (Fig. 7 H and Video 7; separations observed in 16/21 *sqh-AE* and 14/14 *sqh-EE* embryos). These separations involved recoil between Myo-II structures in adjacent cells, resulting in gaps in the supracellular Myo-II meshwork (Fig. 7, H and J). Furthermore, the phenotype of MBS knockdown resembled phosphomimetic Myo-II mutants, also displaying Myo-II separations (Fig. 7, K and L; and Video 7; separations observed in 9/9 *MBS-shRNA* embryos). In the *sqh-TA* mutant we also observed dynamic separation between Myo-II foci in neighboring cells, suggesting that high levels of phosphorylation and/or Myo-II remodeling are important to maintain strong intercellular coupling between actomyosin networks as the tissue invaginates (Fig. 7 I and Video 7; separations observed in 7/15 *sqh-TA* embryos). Although the separation between Myo-II networks in adjacent cells is similar to cytoskeletal separations observed in mutants that reduce cell–cell adhesion (Martin et al., 2010), the *sqh-TA* and *sqh-AE* mutants exhibited normal apical E-cadherin localization (Fig. S5, D–F). Thus, dynamic Myo-II pulses appear to be important for coordinating

apical constriction and the contractile force balance between cells to maintain intercellular cytoskeletal connections in the supracellular actomyosin meshwork that transmits tension across the ventral furrow tissue.

Discussion

Recent studies demonstrated that pulsatile Myo-II contractions drive diverse morphogenetic processes, including *Caenorhabditis elegans* embryo polarization (Munro et al., 2004), *Drosophila* gastrulation (Martin et al., 2009; Roh-Johnson et al., 2012; He et al., 2014), dorsal closure (Blanchard et al., 2010; David et al., 2010; Azevedo et al., 2011), germband extension (Rauzi et al., 2010; Fernandez-Gonzalez and Zallen, 2011; Sawyer et al., 2011), oocyte elongation (He et al., 2010), and *Xenopus laevis* convergent extension (Skoglund et al., 2008; Kim and Davidson, 2011; Shindo and Wallingford, 2014). Although Rok, and likely Myo-II activation via Rok phosphorylation, is required for contraction (Dawes-Hoang et al., 2005; He et al., 2010; Kim and Davidson, 2011; Mason et al., 2013), it was not clear whether Myo-II activation simply regulates cortical Myo-II levels or

whether coupling between Myo-II activity and its regulators organizes contractile pulses in space and time. Furthermore, why cells undergo pulsatile, rather than continuous, contraction to drive tissue morphogenesis was unknown. We were able to answer these questions by visualizing the consequences of uncoupling Myo-II activation from upstream signaling pathways on cell and tissue dynamics.

Dynamic Myo-II phosphoregulation organizes contractile pulses

We identified dynamic Myo-II phosphorylation as a key mechanism that regulates contractile pulses. We found that Myo-II pulses are associated with dynamic medioapical Rok foci and myosin phosphatase. In addition, the phosphomimetic *sqh-AE* and *sqh-EE* mutants, which exhibited constitutive cytoplasmic Myo-II assembly in vivo, exhibited defects in two properties of contractile pulses. First, phosphomimetic mutants did not initially condense apical Myo-II or F-actin into medioapical foci, resulting in Myo-II accumulation across the apical domain and thus a defect in Myo-II radial cell polarity. Second, phosphomimetic mutants continuously accumulated Myo-II in the apical cortex, lacking clear cycles of Myo-II remodeling that are observed in wild-type embryos. Although the phosphomimetic alleles are predicted to partially activate the Myo-II motor's ATPase activity compared with normal phosphorylation (Kamisoyama et al., 1994), the similarity of the MBS knockdown phenotype suggests that the changes in Myo-II organization and dynamics in phosphomimetic mutants reflect defects in the control over Myo-II dynamics rather than a reduction in motor activity. The consequence of persistent Myo-II assembly across the apical surface in phosphomimetic mutants and MBS knockdown is a more continuous, rather than incremental, apical constriction, demonstrating that pulsatile cell shape change results from temporal and spatial regulation of Myo-II activity via a balance between kinase (Rok) and phosphatase (myosin phosphatase) activity.

Mutants that decrease Myo-II phosphorylation affected contractile pulses in a manner that was distinct from the phosphomimetic alleles. Both the *sqh-AA* and the *sqh-TA* mutants exhibited Myo-II assembly into apical foci, potentially mediated by phosphorylation of low levels of endogenous Sqh or phosphorylation of threonine-20, respectively. For the *sqh-TA* mutant, Myo-II assembly was correlated with constriction, suggesting that Myo-II motor activity is not rate limiting to initiate a contractile pulse. However, Myo-II foci in *sqh-TA* and *sqh-AA* mutants were not efficiently remodeled after assembly and coalescence. The persistence of cortical Myo-II foci in *sqh-AA* and *sqh-TA* mutants was surprising given that *rok* mutants and injection of Rok inhibitor reduce cortical localization of Myo-II (Royou et al., 2002, 2004; Dawes-Hoang et al., 2005; Mason et al., 2013). One explanation is that high levels of Myo-II activity induce actomyosin turnover and thus could be required to remodel the actomyosin network after contraction (Murthy and Wadsworth, 2005; Wilson et al., 2010). Alternatively, apical recruitment of myosin phosphatase or proteins that negatively regulate Rok could depend on Myo-II phosphorylation or actomyosin contraction (David et al., 2013). Although future work is needed to address the role of Myo-II motor activity in contractile pulses,

the phenotypes of alleles that constitutively reduce phosphorylation further suggest that cycling between high and low phosphorylation states is required for proper Myo-II pulses.

We propose a model for contractile pulses in the ventral furrow where, in combination with unknown cortical cues that apically localize Myo-II, local pulses of apical Rok activity within the medioapical cortex polarize Myo-II assembly and coalescence (Fig. 8 A). Rok foci could polarize actomyosin condensation by generating an intracellular gradient of minifilament assembly and tension that results in inward centripetal actomyosin network flow (Fig. 8 A, red arrows; Bray and White, 1988; Munro et al., 2004; Mayer et al., 2010). In addition, local Myo-II activation by Rok foci combined with broader myosin phosphatase activity throughout the apical cytoplasm could generate a gradient of Myo-II turnover that will concentrate Myo-II into medioapical foci (Fig. 8 A). MBS is required to restrict phosphorylated Myo-II to specific cell–cell interfaces during dorsal closure, demonstrating that the balance between Myo-II kinases and phosphatase can generate spatial patterns of Myo-II activation in epithelial cells (Mizuno et al., 2002). Myo-II remodeling after coalescence could result from local decreases in Rok activity and enrichment of apical myosin phosphatase with Myo-II structures (Fig. 8 A). Thus, coupling Myo-II activation to dynamic signals that regulate Myo-II phosphorylation organizes contractile pulses in space and time to drive incremental apical constriction.

Polarized actomyosin contraction, pulses, and flows generate force and organize the actin cortex in a variety of cellular and developmental contexts (Lecuit et al., 2011; Salbreux et al., 2012). In contrast to the ratchet-like constriction of ventral furrow cells, some cell types undergo extended periods of actomyosin pulsing and area fluctuations without net reduction in area (Solon et al., 2009; Blanchard et al., 2010; He et al., 2010). Furthermore, directional rearrangement of cell contacts, such as during convergent extension in the *Drosophila* germband, can be achieved through planar polarized accumulation of junctional Rok and Myo-II (Bertet et al., 2004; Blankenship et al., 2006; Simões et al., 2010) in conjunction with planar polarized medioapical actomyosin flows (Rauzi et al., 2010; Levayer and Lecuit, 2013). Modulating the spatial and temporal regulation of Myo-II phosphorylation and dephosphorylation provides a possible mechanism to tune contractile dynamics and organization to generate diverse cell shape changes (Mason and Martin, 2011). Consistent with this organizational role, phosphomimetic RLC mutants also disrupt the planar polarized localization of junctional Myo-II in the *Drosophila* germband (Kasza et al., 2014). Thus, it will be important to define the principles that control Myo-II activity and dynamics and how tuning Myo-II dynamics impacts force generation and tissue movement.

Role of pulsatile Myo-II contractions during tissue morphogenesis

Myo-II phosphomutants resulted in a more continuous apical Myo-II assembly and apical constriction, enabling us to investigate the role of pulsation during tissue morphogenesis. Continuous Myo-II assembly and contraction in the *sqh-AE* mutant resulted in a slower mean rate of apical constriction and thus
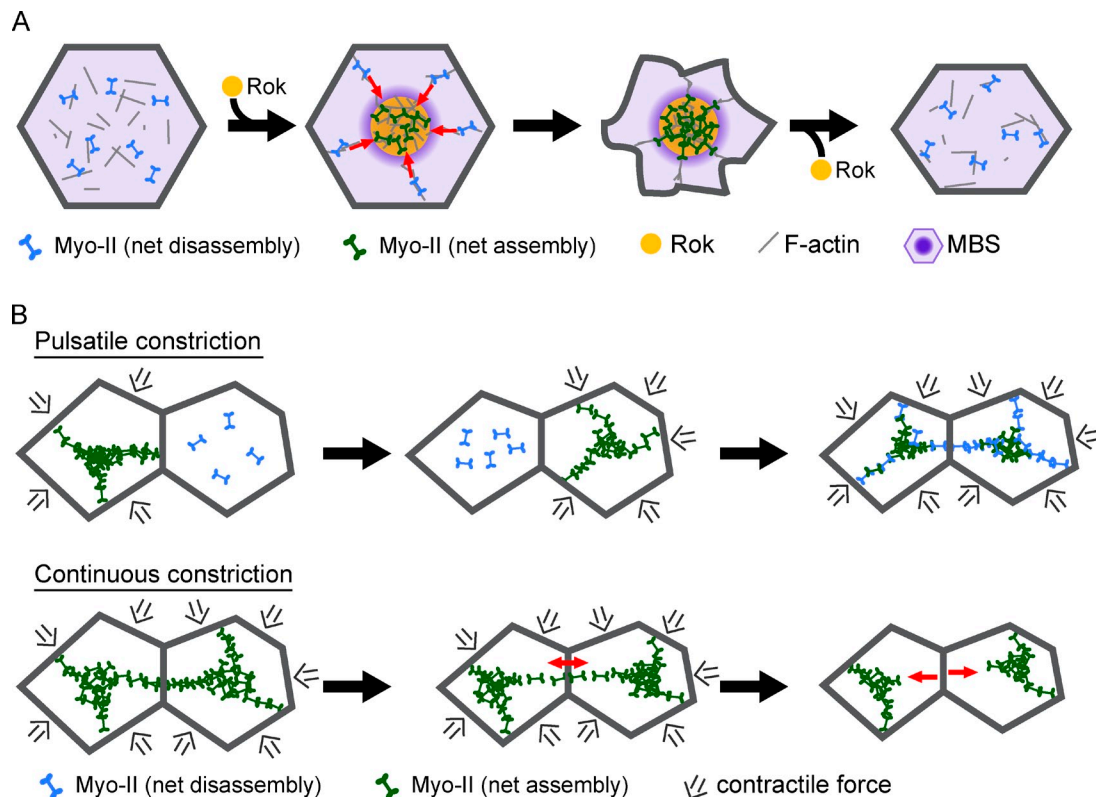
Figure 8. **Model for mechanism and function of contractile pulses.** (A) Myo-II dynamics during a contractile pulse. The contractile pulse is initiated by a local increase in Rok activity that elevates Myo-II phosphorylation and activity. Myo-II coalescence into medioapical foci results from cortical flow (red arrows) resulting from a gradient in cortical tension and net Myo-II minifilament assembly (dark green) at Rok foci with net minifilament disassembly (light blue) in regions of low Rok by myosin phosphatase (purple). Decreased Rok activity after Myo-II coalescence results in Myo-II dephosphorylation followed by remodeling of the contracted cortex. (B) Contractile pulses are required to maintain tissue integrity. Pulsatile Myo-II contraction occurs asynchronously in adjacent cells, which reduces stress at adherens junctions. In addition, Myo-II remodeling allows cells to adjust contacts to maintain stable intercellular cytoskeletal connections. Continuous Myo-II assembly and apical constriction decreases ability of actomyosin networks to dynamically adjust to changes in tissue mechanics, resulting in stretching of Myo-II structures and loss of intercellular connections (red arrows).

delayed tissue invagination. This delay suggested that pulsing might be important for the efficiency of apical constriction. However, phosphomimetic mutants might not fully recapitulate the ATPase activity of phosphorylated Myo-II. The *sqh-TA* mutant, which also perturbs Myo-II remodeling, constricted ventral furrow cells at a rate that is only slightly slower than wild type. In addition, MBS knockdown, which disrupted Myo-II pulses, exhibited a more variable constriction rate, but with a mean rate comparable to control embryos. Our finding is distinct from studies in other cell types where loss of MBS results in excessive phosphorylated Myo-II accumulation and cell invagination (Lee and Treisman, 2004; Corrigall et al., 2007). Thus, MBS can regulate Myo-II organization and dynamics without causing a significant increase in apical Myo-II levels. We conclude that Myo-II pulses are not absolutely required for individual cell apical constriction.

Although phosphomimetic mutant cells constrict and undergo tissue invagination, the coordination of invagination and the stability of the supracellular actomyosin meshwork were perturbed. Continuous apical constriction was associated with abnormal separation events between Myo-II structures in adjacent cells, resulting in gaps or holes in the supracellular Myo-II meshwork. Thus, continuous Myo-II assembly and a lack of Myo-II

dynamics during apical constriction appear to sensitize the tissue to loss of intercellular cytoskeletal integrity during morphogenesis (Fig. 8 B). Although loss of cytoskeletal continuity in phosphomimetic mutants does not block tissue invagination, we speculate that dynamic Myo-II pulses are important to make tissue invagination robust to changes in tensile stress. One possible function of Myo-II pulses is to attenuate tissue tension or stiffness during morphogenetic movements (Fischer et al., 2014). Because pulsed Myo-II contractions are staggered between neighboring cells, pulsation could serve as a mechanism to coordinate contractile force generation across the tissue such that intercellular connections are buffered from high levels of tension (Fig. 8 B). Indeed, reducing adherens junction proteins sensitizes the intercellular connections between cytoskeletal networks to tensile forces generated in ventral furrow cells (Martin et al., 2010; Sawyer et al., 2011; Spahn et al., 2012). Alternatively, remodeling of actomyosin networks that occurs during pulses could be required to adapt the cytoskeletal organization such that forces transmitted between cells accommodate the changing pattern of tissue-scale forces during the course of morphogenesis. In either case, our data suggest that Myo-II pulsing and remodeling are important for collective cell behavior by ensuring proper force transmission between cells in a tissue undergoing morphogenesis.

Materials and methods

Fly stocks and genetics

Stocks used in this investigation are listed in Table S1. Germline clones were generated using the FLP-DFS technique by heat shocking mutant/*ovo*^D larvae for 2 h at 37°C for 3–4 d (Chou and Perrimon, 1992). For two-channel imaging of *Venus::Rok* (UAS-driven; Simões et al., 2010; gift from J. Zallen, Sloan Kettering Institute, New York, NY) and *sqh::mCherry* (sqh promoter), *rok*^2 FRT/FM7;;*mat15 sqh::mCherry*/TM3 females were crossed to *ovo*^D FRT/Y; *hsFlp UAS-Venus::Rok*/CyO males, and embryos from heat shocked *rok*^2 FRT/*ovo*^D FRT; *hsFlp UAS-Venus::Rok*/+; *mat15 sqh::mCherry*/+ females were collected for live imaging. For *sqh::GFP* rescue of *sqh*^1 germline clones, *sqh*^1 FRT/FM7; *sqh-XX::GFP*/CyO females were crossed to *ovo*^D FRT/Y; *hsFlp* males, the resulting larvae were heat shocked, and *sqh*^1 FRT/*ovo*^D FRT; *sqh-XX::GFP*/hsFlp females were crossed to OreR to collect embryos that resulted from germline clones. All *sqh-XX::GFP* transgenes were expressed via the endogenous *sqh* promoter. Sqh phosphomutants were recombined with *Gap43::mCherry* (Memb::Cherry, plasma membrane marker, driven by *sqh* promoter; Martin et al., 2010) or with *Utr::mCherry* (F-actin marker, driven by *sqh* promoter; Rauzi et al., 2010; gift from T. Lecuit, Institut de Biologie du Développment de Marseille, Marseille, France). For *sqh-EE::GFP* suppression of *rok* mutant germline clones, *rok*^1 FRT/FM7; *sqh-EE::GFP*/CyO females were crossed to *ovo*^D FRT/Y; *hsFlp* males and heat shocked. *rok*^1 FRT/*ovo*^D FRT; *sqh-EE::GFP*/hsFlp females were crossed to OreR males to collect embryos. In all cases, control crosses lacking heat shock were performed to verify the presence of the *ovo*^D allele. To generate MBS knockdown embryos, females containing a UAS-driven shRNA against MBS (*MBS-shRNA*) or the *white* gene (control) were crossed to males containing a double-maternal driver line with both *sqh::GFP* and *Gap43::mCherry*. Both UAS stocks were gifts from N. Perrimon, L. Perkins, and the Transgenic RNAi Project (Harvard Medical School, Boston, MA). The resulting larvae were raised at 25°C and females that maternally expressed *MBS-shRNA* or *ctl-shRNA* and both fluorescent markers were crossed to OreR males, and the resulting embryos were imaged.

Construction of GFP-tagged *sqh* phosphomutants

Substitution of threonine-20 and serine-21 with alanine or glutamate prevented or mimicked phosphorylation, respectively (Jordan and Karess, 1997; Winter et al., 2001). The *sqh* gene, including 5′ promoter sequences and 3′ termination sequences, was tagged at the carboxy terminus with eGFP. The *sqh::GFP* sequence is identical to the previously used *sqh::mCherry* construct with the exception of the fluorescent protein sequence (Martin et al., 2009). Site-directed mutagenesis of threonine-20 and/or serine-21 residues was performed on *sqh::GFP* in the pBluescript vector using QuikChange II XL site-directed mutagenesis kit (Agilent Technologies). The 3.5-kb KpnI–XbaI *sqh::GFP* fragments were cloned into the pTiger transformation vector containing an attB site (pTiger courtesy of S. Ferguson, State University of New York at Fredonia, Fredonia, NY). These constructs were sent to Best-Gene Inc. for integration into either the attP1 or attP40 landing sites (see Table S1) using the φC31 integrase system (Groth et al., 2004). Transgenes integrated at these chromosome II landing sites were crossed to the *sqh*^1 mutant. The *sqh-TS::GFP* transgene could rescue *sqh*^1 mutant flies to adulthood; however, homozygous *sqh*^1 adult flies were not observed with any of the *sqh::GFP* phosphomutants (including *sqh-AE* and *sqh-EE*), demonstrating that dynamic myosin phosphorylation is required for development.

Generation of full-length Sqh antibody and Western blotting

Full-length Sqh cDNA was cloned and purified from *E. coli* by GenScript (GenScript USA Inc.). Rabbit sera were obtained using the full-length Sqh as antigen (Panigen, Inc.). Polyclonal anti-Sqh antibody was affinity purified using standard biochemical procedures. In brief, purified Sqh was coupled to CNBr-activated Sepharose 4B (GE Healthcare), the Sqh-coupled resin was incubated with sera, the resin was washed, and the antibody was eluted with glycine, pH 2.5.

Western blotting was performed by grinding embryos directly in sample buffer and running samples on 12% SDS-PAGE gels. Protein was transferred to 0.45-μm nitrocellulose membrane (Bio-Rad Laboratories) and the indicated primary antibodies were detected using horseradish peroxidase–labeled secondary antibodies (Jackson ImmunoResearch Laboratories, Inc.).

Immunohistochemistry

Antibodies and corresponding concentrations used in this investigation are listed in Table S2. For fixed imaging, all embryos were first dechorionated in 50% bleach and then either methanol/heat fixed or PFA fixed. Embryos stained with α-zipper (gift from E. Wieschaus, Princenton University, Princeton,

NJ) and α-neurotactin were methanol/heat fixed (Fig. 3); all other immunostainings used PFA-fixed embryos. For methanol/heat fixations, embryos were placed in boiling Triton salt solution (0.03% Triton X-100 and 0.4% NaCl in water), cooled on ice, and then devitellinized in a 1:1 heptane/methanol solution. PFA-fixed embryos were fixed in a 1:1 solution of 8% PFA in 0.1 M phosphate buffer, pH 7.4, and heptane for 30 min, transferred to a Petri dish, and manually devitellinized using a syringe needle. After immunostaining, heat-fixed embryos were placed on a slide in mounting medium (4% N-propyl-galate in 80% glycerol) and sliced using a syringe blade to create cross sections. PFA-fixed embryos were mounted in AquaPolymount (Polysciences, Inc.). Images were acquired on a confocal microscope (LSM 710; Carl Zeiss) with a 40×/1.2 Apochromat water objective (Carl Zeiss), using argon ion, 561-nm diode, 594-nm HeNe, and 633-nm HeNe lasers. In Figs. 1 and 6, endogenous GFP was used to visualize Myo-II and Rok, respectively.

Time-lapse imaging

Embryos were dechorionated in 50% bleach and mounted ventral side up on a slide coated with "embryo glue" (double-sided tape soaked in heptane). No. 1.5 coverslips were used as spacers and to create a chamber for the mounted embryo. A No. 1 coverslip completes the top of the chamber, and the chamber was filled with Halocarbon 27 oil. All imaging occurred at room temperature (~23°C) on a confocal microscope with a 40×/1.2 Apochromat water objective, argon ion and 561-nm diode lasers, and a pinhole setting between 1 and 2 Airy units. Simultaneous excitation was used for live two-channel imaging of GFP/mCherry or Venus/mCherry. The band-pass filters for Venus/mCherry were set at 519–578 nm and ~599–696 nm, respectively. For Venus/mCherry two-channel imaging, we confirmed that there was minimal spectral bleed-through between channels. The band-pass selected for GFP was ~488–558 nm and for mCherry ~573–696 nm. All images were acquired using Zen software (Carl Zeiss).

Image processing and analysis

Images were processed using Fiji (http://fiji.sc/wiki/index.php/Fiji) and MATLAB (MathWorks).

A Gaussian filter ($\sigma = 0.5$–0.7) was applied to images. Apical images are maximum intensity projections of ~2–5 μm. Subapical image and membrane images are single sections ~1–2 μm below the apical projection.

To quantify Rok and Myo-II intensity over time, we generated kymographs of pulses and acquired intensity values along a linear trace through the kymographs. To determine the phase relationship between Rok and Myo-II signals, a Pearson correlation was calculated for various time offsets where the Rok and Myo-II signals were shifted relative to each other.

We used custom MATLAB software, Embryo Development Geometry Explorer (EDGE; Gelbart et al., 2012), to segment images for quantification of apical area and Myo-II intensities. EDGE automatically segmented cell membranes; however, we manually corrected cells with errors in segmentation. Segmented cell membranes were subapical to the Myo-II signal. Embryos were aligned in time using the mean apical area signals of each embryo by choosing the time where the tissue begins to constrict. For quantification of junctional and medioapical Myo-II intensity in Fig. 4, we used a maximum intensity projection of the raw apical Myo-II signal and applied EDGE to segment images. The medioapical domain of a cell is defined by shrinking the cell's segmented contour by 2 pixels wide; the pixel intensity in this area was used to define medioapical Myo-II, and junctional Myo-II was defined as the difference between the Myo-II intensity in the entire cell and the intensity in the medioapical area (see equations). We then calculated medioapical polarity using the following equations:

$$\text{total Myo-II} = \frac{\sum_{k=1}^{P_T} I_k}{P_T}$$

$$\text{medial Myo-II} = \frac{\sum_{k=1}^{P_m} I_k}{P_m}$$

$$\text{junctional Myo-II} = \frac{\sum_{k=1}^{P_T} I_k - \sum_{k=1}^{P_m} I_k}{P_T - P_m}$$

$$p = \frac{\text{medial Myo-II} - \text{junctional Myo-II}}{\text{total Myo-II}}$$

$$\text{medialapical polarity} = \frac{\sum_{i=1}^{N_c} p_i}{N_c}.$$

P_T = total number of pixels in the cell apex; P_m = number of pixels in the medial region of the cell; I_k = intensity of pixel k; and N_c = number of cells. To quantify Myo-II dynamics in Figs. 5–7, raw Myo-II images were preprocessed to remove cytoplasmic Myo-II by clipping intensity values 2.5 SDs above the mean intensity of cytoplasmic Myo-II. A Gaussian filter was applied (σ = 0.5) and maximum intensity z projections were made for the top two highest intensity values of Myo-II and imported into EDGE. To compare the frequency of instances of rapid Myo-II intensity increase or instances of rapid area reduction between embryos (Fig. 5, D and E; and Fig. 6 G), we first smoothed signals for apical area and mean Myo-II intensity and calculated instantaneous rates for each time point. Rapid Myo-II intensity increases or rapid area reductions were defined as instances where the Myo-II accumulation rate (for Figs. 5 D and 6 G) or the constriction rate (for Fig. 5 E), respectively, exceed a threshold of one SD above the mean rate for all control cells (sqh-TS for Fig. 5 and ctl-shRNA for Fig. 6). To compare maximum constriction rates between control and mutants (Fig. 5 F), we identified the instance of where the constriction rate of each cell was maximal. The identified maximum constriction rates were averaged for control and mutant embryos. The time-resolved cross-correlation between constriction rate and Myo-II accumulation rate (Figs. 5 G and 6 F) was measured by calculating the Pearson correlation between constriction rate and Myo-II accumulation rate for different time offsets. Mean Myo-II intensities displayed in Fig. 7 (A and D) were normalized such that the minimum and maximum intensity values were 0 and 1, respectively. We calculated the mean constriction rate for Fig. 7 (C and F) by taking the negative slope of the apical area between the time apical constriction initiates and 3 min later for each cell.

Statistics
Statistical analyses were performed using the MATLAB statistics toolbox. P-values were calculated using a two-tailed unpaired t test in Figs. 4–7.

Online supplemental material
Fig. S1 shows the characterization of the sqh phosphomutant germline clones before gastrulation and control staining for the MBS knockdown. Fig. S2 shows the sqh phosphomutants during ventral furrow formation. Fig. S3 shows the rok mutant germline clones with sqh-TS or sqh-EE. Fig. S4 shows plots of apical area and Myo-II intensity for individual cells undergoing apical constriction in sqh phosphomutants and MBS knockdown. Fig. S5 shows timing of ventral furrow invagination and E-cadherin staining for sqh phosphomutants. Video 1 is a time-lapse video of embryos expressing Venus::Rok and Sqh::Cherry. Video 2 is a time-lapse video of the sqh phosphomutant embryos during ventral furrow formation. Video 3 is a time-lapse video of embryos expressing GFP-tagged sqh-TS, -TA, or -AE (green) and Utr::mCherry (F-actin). Video 4 is a time-lapse video of rok mutant germline clones expressing sqh-TS or sqh-EE. Video 5 is a time-lapse video of embryos expressing GFP-tagged sqh-TS, -TA, or -AE and Memb::Cherry. Video 6 is a time-lapse video of an embryo depleted of MBS during ventral furrow formation expressing sqh::GFP and Memb::Cherry (membrane). Video 7 is a time-lapse video that highlights intercellular detachments of Myo-II networks in sqh phosphomutants and MBS knockdown. Table S1 lists the genotypes of all of the fly stocks used in this study. Table S2 lists the antibodies and the concentration used for Western blot or immunostaining. Online supplemental material is available at http://www.jcb.org/cgi/content/full/jcb.201402004/DC1.

References

Amano, M., M. Ito, K. Kimura, Y. Fukata, K. Chihara, T. Nakano, Y. Matsuura, and K. Kaibuchi. 1996. Phosphorylation and activation of myosin by Rho-associated kinase (Rho-kinase). J. Biol. Chem. 271:20246–20249. http://dx.doi.org/10.1074/jbc.271.34.20246

Azevedo, D., M. Antunes, S. Prag, X. Ma, U. Hacker, G.W. Brodland, M.S. Hutson, J. Solon, and A. Jacinto. 2011. DRhoGEF2 regulates cellular tension and cell pulsations in the Amnioserosa during Drosophila dorsal closure. PLoS ONE. 6:e23964. http://dx.doi.org/10.1371/journal.pone.0023964

Bardet, P.L., B. Guirao, C. Paoletti, F. Serman, V. Léopold, F. Bosveld, Y. Goya, V. Mirouse, F. Graner, and Y. Bellaïche. 2013. PTEN controls junction lengthening and stability during cell rearrangement in epithelial tissue. Dev. Cell. 25:534–546. http://dx.doi.org/10.1016/j.devcel.2013.04.020

Barrett, K., M. Leptin, and J. Settleman. 1997. The Rho GTPase and a putative RhoGEF mediate a signaling pathway for the cell shape changes in Drosophila gastrulation. Cell. 91:905–915. http://dx.doi.org/10.1016/S0092-8674(00)80482-1

Bertet, C., L. Sulak, and T. Lecuit. 2004. Myosin-dependent junction remodelling controls planar cell intercalation and axis elongation. Nature. 429:667–671. http://dx.doi.org/10.1038/nature02590

Blanchard, G.B., S. Murugesu, R.J. Adams, A. Martinez-Arias, and N. Gorfinkiel. 2010. Cytoskeletal dynamics and supracellular organisation of cell shape fluctuations during dorsal closure. Development. 137:2743–2752. http://dx.doi.org/10.1242/dev.045872

Blankenship, J.T., S.T. Backovic, J.S. Sanny, O. Weitz, and J.A. Zallen. 2006. Multicellular rosette formation links planar cell polarity to tissue morphogenesis. Dev. Cell. 11:459–470. http://dx.doi.org/10.1016/j.devcel.2006.09.007

Bray, D., and J.G. White. 1988. Cortical flow in animal cells. Science. 239:883–888. http://dx.doi.org/10.1126/science.3277283

Bresnick, A.R., V.L. Wolff-Long, O. Baumann, and T.D. Pollard. 1995. Phosphorylation on threonine-18 of the regulatory light chain dissociates the ATPase and motor properties of smooth muscle myosin II. Biochemistry. 34:12576–12583. http://dx.doi.org/10.1021/bi00039a012

Chou, T.B., and N. Perrimon. 1992. Use of a yeast site-specific recombinase to produce female germline chimeras in Drosophila. Genetics. 131:643–653.

Corrigall, D., R.F. Walther, L. Rodriguez, P. Fichelson, and F. Pichaud. 2007. Hedgehog signaling is a principal inducer of Myosin-II-driven cell ingression in Drosophila epithelia. Dev. Cell. 13:730–742. http://dx.doi.org/10.1016/j.devcel.2007.09.015

David, D.J., A. Tishkina, and T.J. Harris. 2010. The PAR complex regulates pulsed actomyosin contractions during amnioserosa apical constriction in Drosophila. Development. 137:1645–1655. http://dx.doi.org/10.1242/dev.044107

David, D.J., Q. Wang, J.J. Feng, and T.J. Harris. 2013. Bazooka inhibits aPKC to limit antagonism of actomyosin networks during amnioserosa apical constriction. Development. 140:4719–4729. http://dx.doi.org/10.1242/dev.098491

Dawes-Hoang, R.E., K.M. Parmar, A.E. Christiansen, C.B. Phelps, A.H. Brand, and E.F. Wieschaus. 2005. folded gastrulation, cell shape change and the control of myosin localization. Development. 132:4165–4178. http://dx.doi.org/10.1242/dev.01938

Fernandez-Gonzalez, R., and J.A. Zallen. 2011. Oscillatory behaviors and hierarchical assembly of contractile structures in intercalating cells. Phys. Biol. 8:045005. http://dx.doi.org/10.1088/1478-3975/8/4/045005

Fischer, S.C., G.B. Blanchard, J. Duque, R.J. Adams, A.M. Arias, S.D. Guest, and N. Gorfinkiel. 2014. Contractile and mechanical properties of epithelia with perturbed actomyosin dynamics. PLoS ONE. 9:e95695. http://dx.doi.org/10.1371/journal.pone.0095695

Gelbart, M.A., B. He, A.C. Martin, S.Y. Thiberge, E.F. Wieschaus, and M. Kaschube. 2012. Volume conservation principle involved in cell lengthening and nucleus movement during tissue morphogenesis. Proc. Natl. Acad. Sci. USA. 109:19298–19303. http://dx.doi.org/10.1073/pnas.1205258109

Groth, A.C., M. Fish, R. Nusse, and M.P. Calos. 2004. Construction of transgenic Drosophila by using the site-specific integrase from phage φC31. Genetics. 166:1775–1782. http://dx.doi.org/10.1534/genetics.166.4.1775

Häcker, U., and N. Perrimon. 1998. DRhoGEF2 encodes a member of the Dbl family of oncogenes and controls cell shape changes during gastrulation in *Drosophila*. *Genes Dev*. 12:274–284. http://dx.doi.org/10.1101/gad.12.2.274

Hartshorne, D.J., M. Ito, and F. Erdödi. 1998. Myosin light chain phosphatase: subunit composition, interactions and regulation. *J. Muscle Res. Cell Motil*. 19:325–341. http://dx.doi.org/10.1023/A:1005385302064

He, B., K. Doubrovinski, O. Polyakov, and E. Wieschaus. 2014. Apical constriction drives tissue-scale hydrodynamic flow to mediate cell elongation. *Nature*. 508:392–396. http://dx.doi.org/10.1038/nature13070

He, L., X. Wang, H.L. Tang, and D.J. Montell. 2010. Tissue elongation requires oscillating contractions of a basal actomyosin network. *Nat. Cell Biol*. 12:1133–1142. http://dx.doi.org/10.1038/ncb2124

Heisenberg, C.-P., and Y. Bellaïche. 2013. Forces in tissue morphogenesis and patterning. *Cell*. 153:948–962. http://dx.doi.org/10.1016/j.cell.2013.05.008

Hildebrand, J.D. 2005. Shroom regulates epithelial cell shape via the apical positioning of an actomyosin network. *J. Cell Sci*. 118:5191–5203. http://dx.doi.org/10.1242/jcs.02626

Jordan, P., and R. Karess. 1997. Myosin light chain–activating phosphorylation sites are required for oogenesis in *Drosophila*. *J. Cell Biol*. 139:1805–1819. http://dx.doi.org/10.1083/jcb.139.7.1805

Kamisoyama, H., Y. Araki, and M. Ikebe. 1994. Mutagenesis of the phosphorylation site (serine 19) of smooth muscle myosin regulatory light chain and its effects on the properties of myosin. *Biochemistry*. 33:840–847. http://dx.doi.org/10.1021/bi00169a027

Karess, R.E., X.J. Chang, K.A. Edwards, S. Kulkarni, I. Aguilera, and D.P. Kiehart. 1991. The regulatory light chain of nonmuscle myosin is encoded by *spaghetti-squash*, a gene required for cytokinesis in *Drosophila*. *Cell*. 65:1177–1189. http://dx.doi.org/10.1016/0092-8674(91)90013-O

Kasza, K.E., D.L. Farrell, and J.A. Zallen. 2014. Spatiotemporal control of epithelial remodeling by regulated myosin phosphorylation. *Proc. Natl. Acad. Sci. USA*. In press.

Kawano, Y., Y. Fukata, N. Oshiro, M. Amano, T. Nakamura, M. Ito, F. Matsumura, M. Inagaki, and K. Kaibuchi. 1999. Phosphorylation of myosin-binding subunit (MBS) of myosin phosphatase by Rho-kinase in vivo. *J. Cell Biol*. 147:1023–1038. http://dx.doi.org/10.1083/jcb.147.5.1023

Kim, H.Y., and L.A. Davidson. 2011. Punctuated actin contractions during convergent extension and their permissive regulation by the non-canonical Wnt-signaling pathway. *J. Cell Sci*. 124:635–646. http://dx.doi.org/10.1242/jcs.067579

Kimura, K., M. Ito, M. Amano, K. Chihara, Y. Fukata, M. Nakafuku, B. Yamamori, J. Feng, T. Nakano, K. Okawa, et al. 1996. Regulation of myosin phosphatase by Rho and Rho-associated kinase (Rho-kinase). *Science*. 273:245–248. http://dx.doi.org/10.1126/science.273.5272.245

Lecuit, T., P.F. Lenne, and E. Munro. 2011. Force generation, transmission, and integration during cell and tissue morphogenesis. *Annu. Rev. Cell Dev. Biol*. 27:157–184. http://dx.doi.org/10.1146/annurev-cellbio-100109-104027

Lee, A., and J.E. Treisman. 2004. Excessive Myosin activity in mbs mutants causes photoreceptor movement out of the *Drosophila* eye disc epithelium. *Mol. Biol. Cell*. 15:3285–3295. http://dx.doi.org/10.1091/mbc.E04-01-0057

Lee, J.Y., and R.M. Harland. 2007. Actomyosin contractility and microtubules drive apical constriction in *Xenopus* bottle cells. *Dev. Biol*. 311:40–52. http://dx.doi.org/10.1016/j.ydbio.2007.08.010

Lee, J.Y., D.J. Marston, T. Walston, J. Hardin, A. Halberstadt, and B. Goldstein. 2006. Wnt/Frizzled signaling controls *C. elegans* gastrulation by activating actomyosin contractility. *Curr. Biol*. 16:1986–1997. http://dx.doi.org/10.1016/j.cub.2006.08.090

Leptin, M. 2005. Gastrulation movements: the logic and the nuts and bolts. *Dev. Cell*. 8:305–320. http://dx.doi.org/10.1016/j.devcel.2005.02.007

Leptin, M., and B. Grunewald. 1990. Cell shape changes during gastrulation in *Drosophila*. *Development*. 110:73–84.

Levayer, R., and T. Lecuit. 2013. Oscillation and polarity of E-cadherin asymmetries control actomyosin flow patterns during morphogenesis. *Dev. Cell*. 26:162–175. http://dx.doi.org/10.1016/j.devcel.2013.06.020

Majumder, P., G. Aranjuez, J. Amick, and J.A. McDonald. 2012. Par-1 controls myosin-II activity through myosin phosphatase to regulate border cell migration. *Curr. Biol*. 22:363–372. http://dx.doi.org/10.1016/j.cub.2012.01.037

Martin, A.C., and B. Goldstein. 2014. Apical constriction: themes and variations on a cellular mechanism driving morphogenesis. *Development*. 141:1987–1998. http://dx.doi.org/10.1242/dev.102228

Martin, A.C., M. Kaschube, and E.F. Wieschaus. 2009. Pulsed contractions of an actin-myosin network drive apical constriction. *Nature*. 457:495–499. http://dx.doi.org/10.1038/nature07522

Martin, A.C., M. Gelbart, R. Fernandez-Gonzalez, M. Kaschube, and E.F. Wieschaus. 2010. Integration of contractile forces during tissue invagination. *J. Cell Biol*. 188:735–749. http://dx.doi.org/10.1083/jcb.200910099

Mason, F.M., and A.C. Martin. 2011. Tuning cell shape change with contractile ratchets. *Curr. Opin. Genet. Dev*. 21:671–679. http://dx.doi.org/10.1016/j.gde.2011.08.002

Mason, F.M., M. Tworoger, and A.C. Martin. 2013. Apical domain polarization localizes actin-myosin activity to drive ratchet-like apical constriction. *Nat. Cell Biol*. 15:926–936. http://dx.doi.org/10.1038/ncb2796

Mayer, M., M. Depken, J.S. Bois, F. Jülicher, and S.W. Grill. 2010. Anisotropies in cortical tension reveal the physical basis of polarizing cortical flows. *Nature*. 467:617–621. http://dx.doi.org/10.1038/nature09376

Mizuno, T., K. Tsutsui, and Y. Nishida. 2002. *Drosophila* myosin phosphatase and its role in dorsal closure. *Development*. 129:1215–1223.

Munro, E., J. Nance, and J.R. Priess. 2004. Cortical flows powered by asymmetrical contraction transport PAR proteins to establish and maintain anterior-posterior polarity in the early *C. elegans* embryo. *Dev. Cell*. 7:413–424. http://dx.doi.org/10.1016/j.devcel.2004.08.001

Murthy, K., and P. Wadsworth. 2005. Myosin-II-dependent localization and dynamics of F-actin during cytokinesis. *Curr. Biol*. 15:724–731. http://dx.doi.org/10.1016/j.cub.2005.02.055

Nance, J., E.M. Munro, and J.R. Priess. 2003. *C. elegans* PAR-3 and PAR-6 are required for apicobasal asymmetries associated with cell adhesion and gastrulation. *Development*. 130:5339–5350. http://dx.doi.org/10.1242/dev.00735

Ni, J.Q., R. Zhou, B. Czech, L.P. Liu, L. Holderbaum, D. Yang-Zhou, H.S. Shim, R. Tao, D. Handler, P. Karpowicz, et al. 2011. A genome-scale shRNA resource for transgenic RNAi in *Drosophila*. *Nat. Methods*. 8:405–407. http://dx.doi.org/10.1038/nmeth.1592

Nishimura, T., and M. Takeichi. 2008. Shroom3-mediated recruitment of Rho kinases to the apical cell junctions regulates epithelial and neuroepithelial planar remodeling. *Development*. 135:1493–1502. http://dx.doi.org/10.1242/dev.019646

Ong, S., C. Foote, and C. Tan. 2010. Mutations of DMYPT cause over constriction of contractile rings and ring canals during *Drosophila* germline cyst formation. *Dev. Biol*. 346:161–169. http://dx.doi.org/10.1016/j.ydbio.2010.06.008

Rauzi, M., P.F. Lenne, and T. Lecuit. 2010. Planar polarized actomyosin contractile flows control epithelial junction remodelling. *Nature*. 468:1110–1114. http://dx.doi.org/10.1038/nature09566

Roh-Johnson, M., G. Shemer, C.D. Higgins, J.H. McClellan, A.D. Werts, U.S. Tulu, L. Gao, E. Betzig, D.P. Kiehart, and B. Goldstein. 2012. Triggering a cell shape change by exploiting preexisting actomyosin contractions. *Science*. 335:1232–1235. http://dx.doi.org/10.1126/science.1217869

Royou, A., W. Sullivan, and R. Karess. 2002. Cortical recruitment of nonmuscle myosin II in early syncytial *Drosophila* embryos: its role in nuclear axial expansion and its regulation by Cdc2 activity. *J. Cell Biol*. 158:127–137. http://dx.doi.org/10.1083/jcb.200203148

Royou, A., C. Field, J.C. Sisson, W. Sullivan, and R. Karess. 2004. Reassessing the role and dynamics of nonmuscle myosin II during furrow formation in early *Drosophila* embryos. *Mol. Biol. Cell*. 15:838–850. http://dx.doi.org/10.1091/mbc.E03-06-0440

Salbreux, G., G. Charras, and E. Paluch. 2012. Actin cortex mechanics and cellular morphogenesis. *Trends Cell Biol*. 22:536–545. http://dx.doi.org/10.1016/j.tcb.2012.07.001

Sawyer, J.M., J.R. Harrell, G. Shemer, J. Sullivan-Brown, M. Roh-Johnson, and B. Goldstein. 2010. Apical constriction: a cell shape change that can drive morphogenesis. *Dev. Biol*. 341:5–19.

Sawyer, J.K., W. Choi, K.C. Jung, L. He, N.J. Harris, and M. Peifer. 2011. A contractile actomyosin network linked to adherens junctions by Canoe/afadin helps drive convergent extension. *Mol. Biol. Cell*. 22:2491–2508. http://dx.doi.org/10.1091/mbc.E11-05-0411

Sellers, J.R. 1991. Regulation of cytoplasmic and smooth muscle myosin. *Curr. Opin. Cell Biol*. 3:98–104. http://dx.doi.org/10.1016/0955-0674(91)90171-T

Shindo, A., and J.B. Wallingford. 2014. PCP and septins compartmentalize cortical actomyosin to direct collective cell movement. *Science*. 343:649–652. http://dx.doi.org/10.1126/science.1243126

Simões, S.M., J.T. Blankenship, O. Weitz, D.L. Farrell, M. Tamada, R. Fernandez-Gonzalez, and J.A. Zallen. 2010. Rho-kinase directs Bazooka/Par-3 planar polarity during *Drosophila* axis elongation. *Dev. Cell*. 19:377–388. http://dx.doi.org/10.1016/j.devcel.2010.08.011

Skoglund, P., A. Rolo, X. Chen, B.M. Gumbiner, and R. Keller. 2008. Convergence and extension at gastrulation require a myosin IIB-dependent cortical actin network. *Development*. 135:2435–2444. http://dx.doi.org/10.1242/dev.014704

Solon, J., A. Kaya-Copur, J. Colombelli, and D. Brunner. 2009. Pulsed forces timed by a ratchet-like mechanism drive directed tissue movement during dorsal closure. *Cell*. 137:1331–1342. http://dx.doi.org/10.1016/j.cell.2009.03.050

Spahn, P., A. Ott, and R. Reuter. 2012. The PDZ-GEF protein Dizzy regulates the establishment of adherens junctions required for ventral furrow formation in *Drosophila*. *J. Cell Sci.* 125:3801–3812. http://dx.doi.org/10.1242/jcs.101196

Sun, Y., Y. Yan, N. Denef, and T. Schüpbach. 2011. Regulation of somatic myosin activity by protein phosphatase 1β controls *Drosophila* oocyte polarization. *Development*. 138:1991–2001. http://dx.doi.org/10.1242/dev.062190

Sweeton, D., S. Parks, M. Costa, and E. Wieschaus. 1991. Gastrulation in *Drosophila*: the formation of the ventral furrow and posterior midgut invaginations. *Development*. 112:775–789.

Tan, C., B. Stronach, and N. Perrimon. 2003. Roles of myosin phosphatase during *Drosophila* development. *Development*. 130:671–681. http://dx.doi.org/10.1242/dev.00298

Wheatley, S., S. Kulkarni, and R. Karess. 1995. *Drosophila* nonmuscle myosin II is required for rapid cytoplasmic transport during oogenesis and for axial nuclear migration in early embryos. *Development*. 121:1937–1946.

Wilson, C.A., M.A. Tsuchida, G.M. Allen, E.L. Barnhart, K.T. Applegate, P.T. Yam, L. Ji, K. Keren, G. Danuser, and J.A. Theriot. 2010. Myosin II contributes to cell-scale actin network treadmilling through network disassembly. *Nature*. 465:373–377. http://dx.doi.org/10.1038/nature08994

Winter, C.G., B. Wang, A. Ballew, A. Royou, R. Karess, J.D. Axelrod, and L. Luo. 2001. *Drosophila* Rho-associated kinase (Drok) links Frizzled-mediated planar cell polarity signaling to the actin cytoskeleton. *Cell*. 105:81–91. http://dx.doi.org/10.1016/S0092-8674(01)00298-7

Young, P.E., T.C. Pesacreta, and D.P. Kiehart. 1991. Dynamic changes in the distribution of cytoplasmic myosin during *Drosophila* embryogenesis. *Development*. 111:1–14.